applied sciences

MDPI

Article

An Improved Approach for Atrial Fibrillation Detection in Long-Term ECG Using Decomposition Transforms and Least-Squares Support Vector Machine

Tomasz Pander

Department of Cybernetics, Nanotechnology and Data Processing, Faculty of Automatic Control, Electronics and Computer Science, Silesian University of Technology, Akademicka 16, 44-100 Gliwice, Poland; tpander@polsl.pl; Tel.: +48-32-237-15-63

Abstract: Atrial fibrillation is a common heart rhythm disorder that is now becoming a significant healthcare challenge as it affects more and more people in developed countries. This paper proposes a novel approach for detecting this disease. For this purpose, we examined the ECG signal by detecting QRS complexes and then selecting 30 successive R-peaks and analyzing the atrial activity segment with a variety of indices, including the entropy change, the variance of the wavelet transform indices, and the distribution of energy in bands determined by the dual-Q tunable Q-factor wavelet transform and coefficients of the Hilbert transform of ensemble empirical mode decomposition. These transformations provided a vector of 21 features that characterized the relevant part of the electrocardiography signal. The MIT-BIH Atrial Fibrillation Database was used to evaluate the proposed method. Then, using the *K*-fold cross-validation method, the sets of features were fed into the LS-SVM and SVM classifiers and a trilayered neural network classifier. Training and test subsets were set up to avoid sampling from a single participant and to maintain the balance between classes. In addition, individual classification quality scores were analyzed for each signal to determine the dependencies of the classification quality on the subject. The results obtained during the testing procedure showed a sensitivity of 98.86%, a positive predictive value of 99.04%, and a classification accuracy of 98.95%.

Keywords: atrial fibrillation; ECG processing; dual-Q tunable-Q wavelet transform; EEMD; MODWT; LS-SVM classifier

check for updates

Citation: Pander, T. An Improved Approach for Atrial Fibrillation Detection in Long-Term ECG Using Decomposition Transforms and Least-Squares Support Vector Machine. *Appl. Sci.* **2023**, *13*, 12187. https://doi.org/10.3390/app132212187

Academic Editors: Agnese Sbrollini and Aurora Saibene

Received: 22 October 2023
Revised: 5 November 2023
Accepted: 7 November 2023
Published: 9 November 2023

Copyright: © 2023 by the author. Licensee MDPI, Basel, Switzerland. This article is an open access article distributed under the terms and conditions of the Creative Commons Attribution (CC BY) license (https://creativecommons.org/licenses/by/4.0/).

1. Introduction

Cardiovascular disease is the leading cause of death worldwide and is a significant cause of declining health and excessive costs to the health system. According to the global ranking of deaths from cardiovascular causes, atrial fibrillation and atrial flutter are among the top ten reasons [1]. This trend is expected to increase significantly as the population ages [2]. Atrial fibrillation is the most common and invasive heart rhythm disorder worldwide, significantly impacting morbidity and mortality. AF detection is crucial as this cardiac arrhythmia is a well-known risk factor for ischaemic stroke, demonstrating rates up to six times higher than among patients without arrhythmia [3,4]. The early diagnosis and treatment of this heart disease can improve the standard of living and have a long-term impact on people's lives.

Atrial fibrillation describes abnormal heart behavior, which can be symptomatic or asymptomatic and is caused by inappropriate activity within the atria, which in turn causes an irregular ventricular pace. Four different classes of atrial fibrillation can be distinguished in general. The American Heart Association suggests the categorization of AF into first detection, paroxysmal, persistent, and permanent based on the temporal rhythm due to its simplicity and clinical relevance [5]. Identifying AF in a timely manner is critical to prevent life-threatening situations, but it can be challenging, especially for

early-stage AF, also known as paroxysmal AF (PAF) [5,6]. The electrical signal waveform of a single episode of each type of AF is essentially the same. Irregular and inconsistent RR intervals, the presence of a continuous and time-varying atrial fibrillatory signal instead of P-waves, and widening/shrinking in some cases of QRS complexes or fluctuating waveforms in the baseline ECG are the main factors visible in the ECG signal that indicate atrial fibrillation and differentiate it from normal sinus rhythm [5–9]. In the case of AF occurrence, the original P-waves vanish and are replaced by a series of irregular high-frequency oscillations called F-waves. The frequency range in which changes in the signal resulting from the occurrence of AF are recorded is 2–9 Hz [9,10].

1.1. Review of Existing Literature

Remarkable advances in computing power have been achieved, and the latest developments in deep learning technologies have revolutionized the healthcare sector and medical practice. The growing accessibility of wearable gadgets that can monitor pulse and blood oxygen saturation or even capture a single-lead ECG makes it possible to collect data on the functioning and well-being of the heart. Wearable devices, especially in terms of their ECG signal monitoring capabilities combined with AI methods, are already gaining popularity [11]. Personal ECG devices such as the AliveCor Kardia, Apple Watch, or Samsung Galaxy Watch allow one to detect various arrhythmias on a larger scale than ever before and in a non-ambulatory environment [12]. The work of Mäkynen et al. [13] discussed the possibility of applying wearable devices for AF detection, focusing on the benefits and limitations of pairing wearable devices with machine learning/deep learning algorithms.

The electrocardiogram is a fundamental tool for the clinical diagnosis of atrial activity and the assessment of the heart's electrical behavior. By recording and analyzing the electrical signals within the human body, the ECG provides a reliable and non-invasive method for assessing cardiac function and detecting abnormalities [4,8,14]. Non-ECG-based measurements, such as blood pressure, are also feasible, as Verberk et al. [15] demonstrated the ability to obtain a recall of 98% and a specificity of 92% in detecting AF using a blood pressure monitor. Another possibility is the use of a photoplethysmographic signal [16,17], which has achieved a sensitivity and specificity of, respectively, 97% (±3%) and 99% (±3%) [16], or even cardiac dynamics signals, such as the ballistocardiogram signal or the seismocardiogram signal [18].

However, most reports in the literature on AF detection are based on the ECG signal. Hirsch et al. [8] presented an interesting and valid concept for dividing AF detection methods into four groups. These groups of methods were: (i) AF detection based only on the RR interval features [4,19–23], (ii) AF detection based only on the atrial activity (AA) features [2,24,25], (iii) AF detection based on the combination of the RR intervals and the AA features [8,26], and (iv) AF detection based on no manually crafted features from the ECG [7,27–31]. The most significant publications are also presented in the last table of this paper, which displays the results obtained using the MIT-BIH atrial fibrillation reference benchmark database.

Different methods have been used to determine the characteristics of the RR intervals and atrial activity in the ECG signal. One of them is based on estimating the changes in the interval between two consecutive R-waves (RR) with various irregularity measures. The others are based on observing a lack of or abnormal P-waves (replaced by rapid, irregular, and disordered fibrillatory waves, called F-waves) [2,32]. It can be concluded that the absence of P-waves is a crucial indicator of the presence of AF [6]. The occurrence of P-waves makes many methods such as the wavelet transform (WT) [2,24,25] or empirical mode decomposition (EMD) [33,34] useful for the creation of feature sets. Asgari et al. [25] calculated the peak-to-average power ratio and log-energy entropy for each wavelet coefficient. An interesting approach was proposed by Giraldo-Guzmán et al. [7]. It was based on the operation of spatio-temporal filtering to magnify and detect the prominent spatio-temporal patterns within the P-waves in multichannel ECG recordings. In the work of Rahul et al. [35], the ECG signal and its time–frequency representation were regarded

as an image, and for the detection of AF, the bidirectional long- and short-term memory network was applied.

The ability to accurately assess RR intervals provides many benefits, including the capacity for long-term monitoring [32], as well as the ability to use different parameters, such as those used to evaluate fetal heart rate [4]. An interesting approach is the use of non-linear entropy coefficients in the description of RR intervals [8] or discrete-state Markov models [22]. The non-linear fractal dimension (FD) helps discriminate between physiological and pathological ECG [36]. An audio-inspired technique was proposed in [37]. It involved extracting RR-value sequences from filtered ECG signals and applying various audio spectral characteristics to these sequences. The resulting input vectors were then used with different types of manifold estimators. The authors also employed least absolute shrinkage and selection operator (LASSO) regression, a feature selection technique. Such an approach showed that spectral representations of AF segments can induce better-defined low-dimensional embedding manifolds and a sufficient intrinsic separability of AF from sinus rhythm.

It is only sometimes feasible to directly compare previously proposed techniques due to the use of different databases of ECG signals. Artificial intelligence, such as deep learning or machine learning approaches, has significantly impacted the advancement in AF detection methods. A frequently used classifier in AF detection methods is the support vector machine (SVM) classifier [4,19,20,25,26], as well as the K-nearest neighbor (KNN) classifier [38]. A simple linear classifier was used on heart rhythm data in [32]. In ref. [3], the detection of AF was based on the receiver operating characteristic (ROC), which allowed the authors to estimate the optimal threshold for discriminating between episodes of AF and non-AF. A model combining convolutional and recurrent neural networks was proposed to extract high-level features from segments of RR intervals (RRIs) in order to classify them as AF or normal sinus rhythm in ref. [27]. The features of an ECG were extracted by a convolutional neural network (CNN) and loaded into a long short-term memory (LSTM) model in ref. [39]. The work of Staffini et al. [40] paired a variational auto-encoder (VAE) with a bidirectional long short-term memory network (BiLSTM) back end to perform unsupervised anomaly detection on heart rate sequences acquired from wearable devices, obtaining better results than typically used anomaly detection methods. Nurmaini coupled a discrete wavelet transform (DWT) with one-dimensional convolutional neural networks (1D-CNNs) to classify three categories: normal sinus rhythm (NSR), AF, and non-AF [41]. A lightweight CNN-based AF event detector was presented in ref. [42]. The accurate adjustment of the CNN parameters achieved promising AF detection results. The optimization of the parameter values made it possible to run the classification on a Raspberry Pi computer. A combination of atrial activity characteristics and RR interval characteristics was used as input for three popular classifiers (boosted trees (BoT), random forest (RF), and linear discriminant analysis (LDA)) with the random subspace method (RSM) in ref. [8]. Plesinger et al. [43] used statistical descriptions of RR intervals to train a custom 2-layer neural network (NN) and a bagged tree ensemble (BT), while Kamaleswaran et al. [44] applied a 13-layer one-dimensional CNN. Ref. [45] described five well-known pre-trained convolutional neural networks, namely AlexNet, VGG16, GoogLeNet, RenNet50, SqueezeNet, and ShuffleNet, applied to atrial fibrillation detection. The authors verified the detection quality in proprietary and PhysioNet/CinC Challenge 2017 databases. Zhang et al. [46] proposed a dual-domain attention cascade, D2AFNet, for accurate and interpretable AF detection by cascading attention-based bidirectional gated recurrent units and densely connected networks embedded with channel–spatial information fusion modules.

1.2. Proposed Work and Contribution

Numerous studies have been published on the use of machine learning methods for AF detection [4–6,8,14,23,47]. Most of them reported almost perfect quality indicators for AF detection. Researchers have applied different techniques to find the characteristics of

AF. What impact do various characteristics have on the effectiveness of AF detection? Does using characteristics derived from heart rate provide a more effective result than features obtained from electrocardiogram signal examination? To answer these questions, three different signal transformations were applied to obtain an accurate description of the AF phenomenon and learn the selected classifiers.

This paper presents an improved technique for automatically detecting atrial fibrillation and an assessment of its performance. The proposed algorithm considers the part of the ECG signal originating from atrial activity and the heart rate in the range of specified consecutive heartbeats. For this reason, the feature window gathers different kinds of information from 30 heartbeats without overlapping. The first step of the proposed method is pre-processing, which includes, among other things, signal filtering followed by a feature vector extraction step. Several parameters are applied to describe atrial activity in the ECG signal and heart rhythm.

The novel approach is intended for the analysis of AA. The processing of AA is carried out with the dual-Q tunable Q-factor wavelet transform (DQ-TQWT), ensemble empirical mode decomposition (EEMD), and the maximal overlap discrete wavelet transform (MODWT) multiscale variances. DQ-TQWT-based features have never been used in the past for AF detection. These treatments provide the parameter values that are included in the feature vector. Several other parameters are also explored, among which it is worth mentioning the Higuchi fractal dimension and various types of entropy, which are known to be effective in AF detection. In the last step, feature selection is carried out to obtain the best performance and reduce the number of features. The genetic algorithm is used with the wrapper method to optimize feature selection for the highest accuracy. Finally, the LS-SVM method is applied for classification purposes. The proposed method outperforms many contemporary techniques developed in this field. The significant contributions of this paper are as follows:

- The decomposition of part of the ECG signal with the dual-Q tunable Q-factor wavelet transform (DQ-TQWT), ensemble empirical mode decomposition (EEMD), and the corresponding analysis of variances from the maximal overlap discrete wavelet transform (MDDWT);
- The proposal of a differentiated set of features describing atrial activity in the ECG signal and heart rhythm;
- The application of a least-squares support vector machine for classification purposes;
- Experimental results showing that the proposed method's performance in detecting AF episodes was superior to that of state-of-the-art methods.

The paper is organized as follows. The proposed method is presented in Section 2. Section 3 describes the dataset used and presents the experimental results of the proposed method. Section 4 discusses the results obtained. Finally, the conclusions and suggested future research are presented in Section 5.

2. Materials and Methods

A block diagram of the proposed method is shown in Figure 1. It consists of five major stages: (i) the pre-processing stage, which includes denoising and R-peak detection; (ii) atrial activity analysis, which comprises three transformations of the atrial activity extracted from the ECG signal; (iii) heart rhythm analysis; (iv) the gathering of data for the feature vectors; and (v) the classification stage, which includes training (to create a classification model) and testing. The implemented feature estimation methods are all inherently finite or possess stopping criteria to avoid latency or runtime errors. With a data window width of 30 beats [8], the window is marked with a pre-trained classifier. On this basis, the beginning of an episode of atrial fibrillation can be detected with a latency of 30 heartbeats.

The initial pre-processing step aims to reduce the wandering baseline in the ECG signal. Additionally, since raw ECG signals are frequently contaminated by various types of noise, such as muscle noise and 50/60 Hz power line interference, Savitzky–Golay filtering is

used. Subsequently, R-peak detection is performed, for which different algorithms can be used [48]. The detected R-peaks are the basis for calculating the RR interval. RR_i variations between heartbeats reflect both the vagal and sympathetic modulation of the heart sinus node and are commonly used to perform heart rate variability (HRV) analysis. Knowing RR_i, the instantaneous heart rate values HR_i (bpm) are computed. The results of the first stage of the presented method are illustrated in Figure 2. As mentioned in ref. [8], 30 beats are considered to guarantee stable feature extraction, especially for dynamic complexity description factors [49]. The part of the ECG signal that contains these successive QRS complexes is analyzed by the variance of the MODWT, the energy of the corresponding components of the DQ-TQWT, and ensemble EMD transformations.

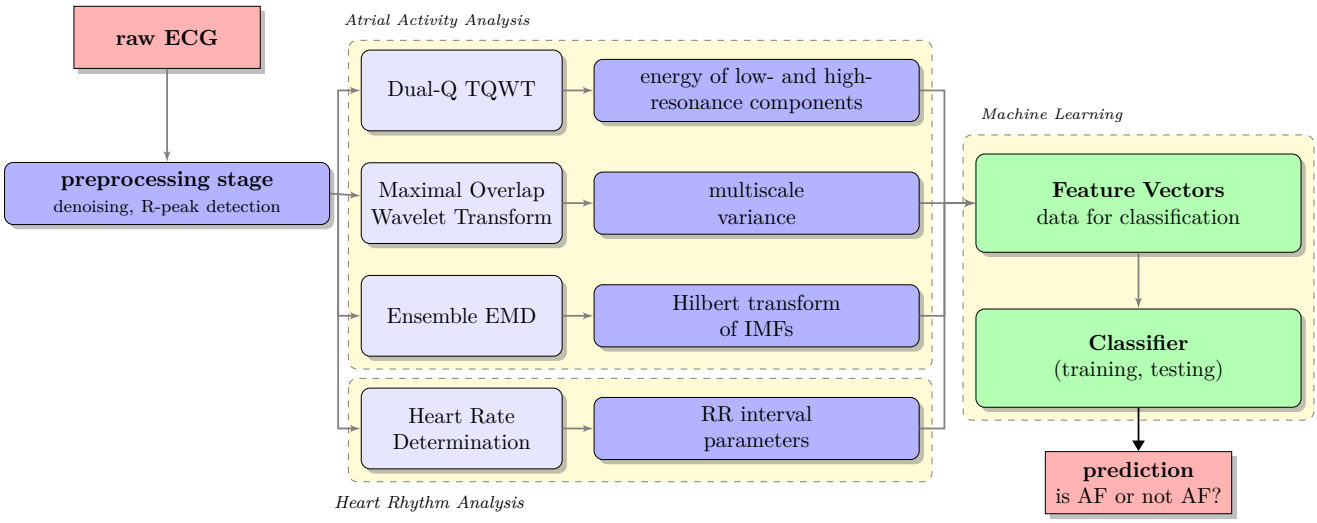

Figure 1. An overview of the proposed algorithm, focusing on the part corresponding to the preparation of the feature vector for the classifier.

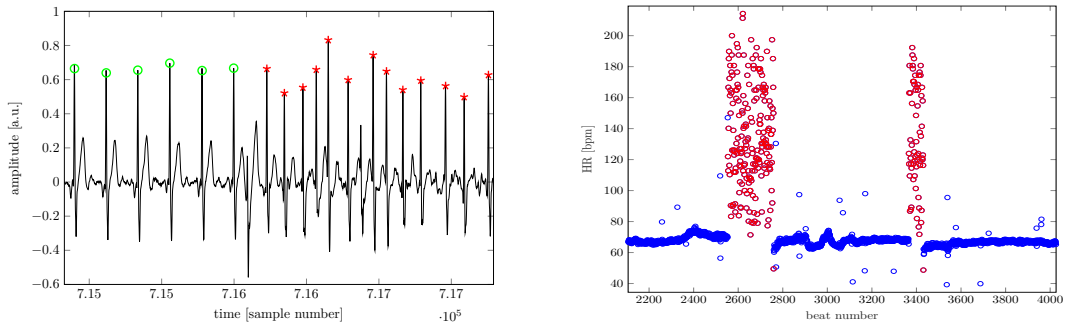

(**a**) ECG signal (**b**) heart rate

Figure 2. (**a**) ECG signal and fibrillation episode in 4048 signal (channel: 1) from MIT-BIH Atrial Fibrillation Database (green circles denote R-peaks with normal sinus rhythm, red stars denote R-peaks annotated as atrial fibrillation); (**b**) heart rate signal (bpm) with clinically recognized AF (blue circles denote normal sinus rhythm heart rate, whereas red circles denote heart rate corresponding to AF).

2.1. Atrial Activity Assessment Factor Extraction

The primary purpose of this stage of the proposed method is to extract the significant features that make the investigated phenomenon distinguishable from the normal activity of the heart. Thanks to the DQ-TQWT, MODWT, and EEMD transformations applied for the indicated part of the ECG signal, in the location where the P-wave appears, it is possible to decompose the signal into components that allow these features to be distinguished.

As well as the FD, complexity characteristics and different types of entropy are calculated to describe atrial activity directly from the ECG signal [8].

According to the work of Hirsh et al. [8], a constant-length window of 0.26 s (starting 0.38 s before the detected R-peak) is used to extract the respective P-wave. An example of atrial activity annotated in the ECG signal is presented in Figure 3. However, it is quite likely that in the case of a high heart rate, the analyzed segment of the ECG signal will also include part of the T-wave. Such a selection allows for the analysis of the part of the ECG that corresponds to the P-wave and omits the QRS complex. In the case of a sampling frequency of 250 Hz, the selected data window consists of 64 samples. As mentioned above, a signal window consisting of thirty R-peaks is analyzed. For each of the RR intervals, each segment of atrial activity is analyzed. Finally, the resulting feature values form the corresponding 30-element vectors, which are then averaged.

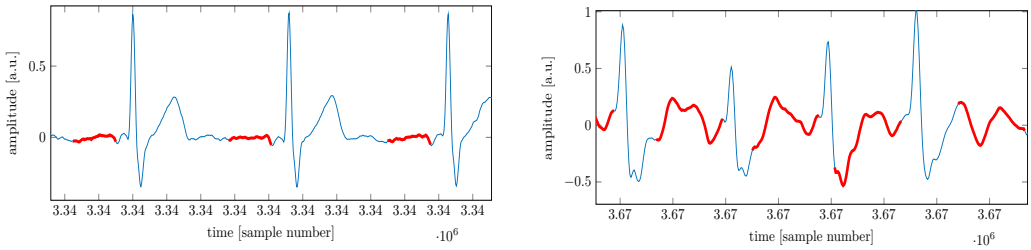

(**a**) (**b**)

Figure 3. Examples of atrial activity (thick red line) without (**a**) and with (**b**) atrial fibrillation (signal 4048 from MITBIH AFDB).

2.2. Dual-Q Tunable Q-Factor Wavelet Transform

Since atrial fibrillation can exhibit some oscillatory characteristics, we decided to use a tunable wavelet transform, which would allow the observation of oscillatory and transient components of the ECG signal in different frequency sub-bands. The tunable Q-factor wavelet transform (TQWT) is a type of WT that can decompose a signal into multiple sub-bands. Using the inverse TQWT, the signal can then be reconstructed from the sub-bands with the highest energy [50]. The traditional WT is characterized by the invariant Q-factor, i.e., the constant ratio of its center frequency to its bandwidth [51]. The operation of the TQWT relies on the combination of three essential parameters: the Q-factor (Q), redundancy (r), and level of decomposition (J). It is imperative to have prior knowledge of these parameters before performing TQWT decomposition. The Q-factor significantly impacts the wavelet's oscillatory behavior, whereas the redundancy r is calculated as the total number of wavelet coefficients divided by the signal length to be used for the TQWT. The value of J is the level of two-channel filter banks that attach to the low-pass filter output, resulting in sub-bands $J+1$ [50,52]. The application of the dual-Q TQWT includes the simultaneous use of the two Q-factors of the WT and was first introduced in [51,53]. This transformation decomposes the signal $\mathbf{x}$ into two components, $\mathbf{x}_1$ and $\mathbf{x}_2$, where $\mathbf{x}_1$ mainly consists of sustained oscillations and $\mathbf{x}_2$ mainly consists of non-oscillatory transients [52]. Let TQWT_1 and TQWT_2 denote the TQWT with two different Q-factors (high and low Q-factors); then, the decomposition of $\mathbf{x}$ can be derived by solving an optimization problem with constraints in the sub-band-dependent regularization form [51]:

$$\arg\min_{\mathbf{w}_1,\mathbf{w}_2} \sum_{j=1}^{J_1+1} \lambda_{1,j}||\mathbf{w}_{1,j}||_1 + \sum_{j=1}^{J_2+1} \lambda_{2,j}||\mathbf{w}_{2,j}||_1, \quad (1)$$

such that

$$\mathbf{x} = \mathrm{TQWT}_1^{-1}(\mathbf{w}_1) + \mathrm{TQWT}_2^{-1}(\mathbf{w}_2), \quad (2)$$

where $\mathbf{w}_{i,j}$ denotes wavelet coefficients of TQWT_i for $i = 1, 2$, and TQWT^{-1} is the inverse transform. To start the decomposition, knowledge of six parameters is required: Q_1, r_1, and

J_1 for the high-Q-factor TQWT and Q_2, r_2, and J_2 for the low-Q-factor TQWT. According to ref. [52], to protect against the problem of wavelet ringing, the parameter r should be greater than or equal to 3. The high-resonance and low-resonance components of the $\mathbf{w}_1$ and $\mathbf{w}_2$ sub-bands are used for further analysis. The percentage of energy from each sub-band is determined on the basis of $\mathbf{w}_1$ and $\mathbf{w}_2$ according to

$$E_{i,j} = \sum_{j=1}^{J_i+1} |w_{i,j}|^2, \tag{3}$$

where J_i is the decomposition level of the TQWT. Then, the peak and average energy, respectively, are estimated as

$$E_{i,peak} = \max_{1 \le j \le J+1} (E_{i,j}) \tag{4}$$

and

$$E_{i,ave} = \text{mean}(E_{i,j})|_{j=1}^{J_i+1}. \tag{5}$$

Finally, two factors are calculated as the ratio of the peak energy to the average energy for high- and low-resonance components, respectively, according to

$$\zeta_i = \frac{E_{i,peak}}{E_{i,ave}}, \tag{6}$$

where $i = 1, 2$.

Having obtained the wavelet coefficients $\mathbf{w}_{1,2}$ with the DQ-TQWT, the wavelet entropy is also calculated as the maximum entropy value in individual sub-bands for the high- and low-resonance components of the transformation. WT-based entropy measures the degree of both order and disorder in a signal, as well as the underlying dynamic process associated with it. The Matlab procedure *wentropy* (Shannon entropy) is applied, and the corresponding factors are indicated as $E_{\mathbf{w}1}$ and $E_{\mathbf{w}2}$, respectively, for high- and low-resonance decomposition coefficients after the DQ-TQWT. The energy distribution within the sub-bands for high- and low-resonance components is presented in Figure 4.

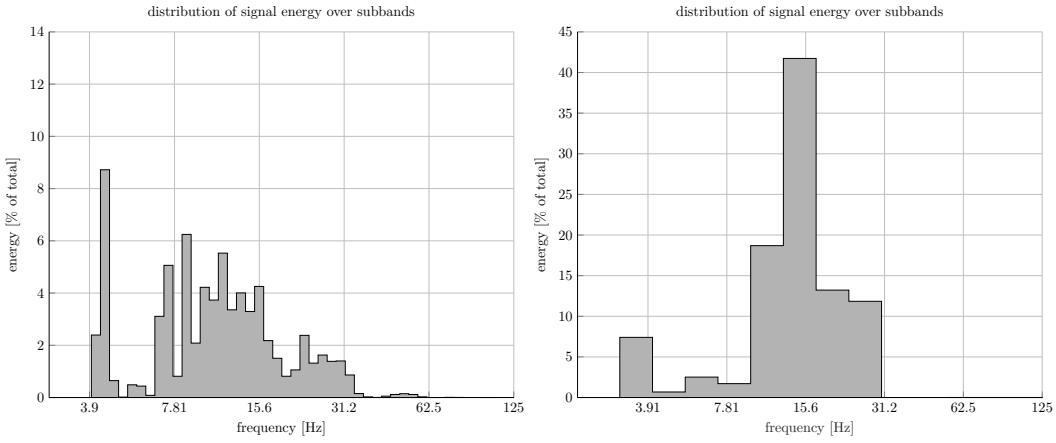

(**a**) The NSR case (high-resonance components). (**b**) The NSR case (low-resonance components).

Figure 4. *Cont.*

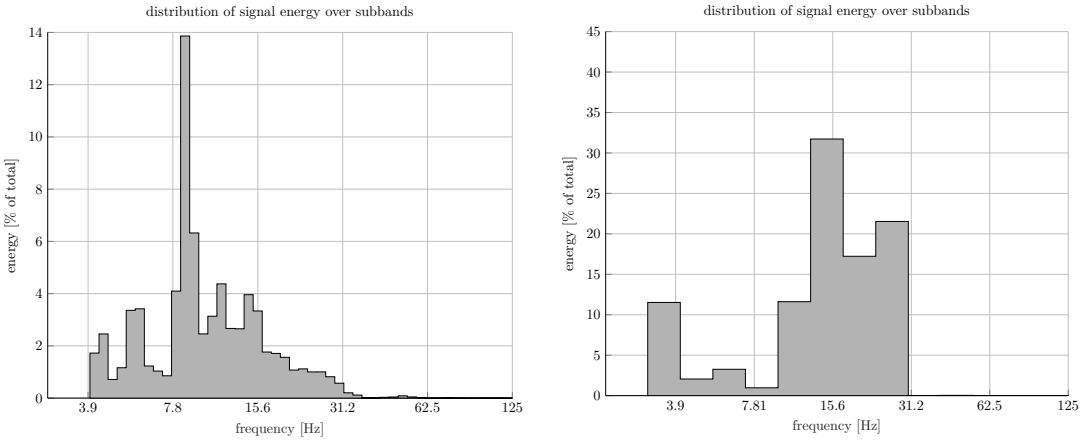

(**c**) The AF case (high-resonance components). (**d**) The AF case (low-resonance components).

Figure 4. Different energy distributions within sub-bands in wavelet coefficient domain for normal sinus rhythm (NSR) (**a**,**b**) and for atrial fibrillation (**c**,**d**).

2.3. The Variance of the Maximal Overlap Discrete Wavelet Transform

The absence of a typical P-wave characterizes an ECG signal that contains episodes of AF. This fact affects the energy distribution in that signal. For this reason, maximal overlap discrete wavelet transformation is applied to the atrial activity signal to identify the absence of a common P-wave component in the ECG signal. MODWT preserves energy; it is well suited to analyzing the dependence of variation on scale in ANOVA studies. The examination of wavelet variance permits the identification of the scales that are most significant in the general variability of the data. In addition, MODWT can be used as a variance estimator [54]. This transformation resolves the issue of the time variance property, promoting no downsampling. That is, all MODWT decomposition layers maintain the exact time resolution without phase distortion [55]. MODWT enhances the alignment of the decomposed wavelet and scaling coefficients at an individual level with the original time series. This transform aligns the wavelet coefficients at each time range with the original signal. The calculated variances $\hat{v}_j^2$ allow the analysis of the localized signal variation with respect to scale and time [56]. To apply MODWT to a finite time-series signal $x(n)$ and decompose it into J levels, J pairs of wavelet (high-pass) $\tilde{h}_{j,l}$ and scaling (low-pass) filters $\tilde{g}_{j,l}$ must be used. At the j-th level, a filtering operation is performed to obtain a set of wavelet and scaling coefficients, as described in ref. [54]:

$$\bar{W}_{j,n} = \sum_{l=1}^{L_j-1} \tilde{h}_{j,l} x(n-l), \tag{7}$$

$$\bar{V}_{j,n} = \sum_{l=1}^{L_j-1} \tilde{g}_{j,l} x(n-l), \tag{8}$$

where $n = 0, 1, \ldots, N-1$, and $\tilde{h}_{j,l}$ and $\tilde{g}_{j,l}$ are the j-th level MODWT wavelet and scaling filters, respectively. The variance estimate is defined as

$$\hat{v}_j^2 = \frac{1}{L_j} \sum_{l=1}^{L_j-1} \bar{W}_{j,n}^2. \tag{9}$$

In this work, the Matlab procedures *modwt* and *modwtvar* are used, and $\hat{v}_j^2$ denotes the variances obtained. Variances $\hat{v}_j^2$ $(j = 1, \ldots, 9)$ are calculated for the first nine levels of decomposition.

2.4. Ensemble Empirical Mode Decomposition

Empirical mode decomposition (EMD) was introduced by Huang et al. in ref. [57]. A variation of EMD is the ensemble EMD (EEMD), which decomposes the original signal over an ensemble of noisy copies and obtains the final results by averaging. White noise can provide a uniformly distributed scale in the time–frequency domain. The EEMD algorithm can be described as follows [58]:

1. Generate $x(n)^{(m)} = x(n) + \beta \cdot w^{(m)}$, where $w^{(m)}$, $m = 1, \ldots, K$ are different realizations of white noise and $x(n)$ is the atrial activity signal (P wave);
2. Decompose each $x(n)^{(m)}$, $m = 1, \ldots, K$ completely by EMD, obtaining its modes $c_i^{(m)}$, where $i = 1, \ldots, M$ indicates modes and K is the so-called ensemble number;
3. Assign $\bar{c}_i$ as the ith mode (IMF) of $x(n)$, obtained by averaging the corresponding modes.

It should be mentioned that in EEMD, each $x(n)^{(m)}$ is decomposed independently of the different noise realizations, and for each of them, a residual $r(n)$ is obtained at each stage. Having obtained the intrinsic mode function components from the EEMD, the Hilbert transform is applied to each IMF component [59]. This transform allows one to obtain one of the instantaneous amplitudes (InAs—the absolute values of the analytic signals) [8]. Taking into account the ith IMF and applying the Hilbert transform, the respective analytic signal, $x_i^a(n)$, is calculated as

$$x_i^a(n) = \mathrm{IMF}_i + \mathrm{j} \cdot \mathcal{H}(\mathrm{IMF}_i), \tag{10}$$

where $\mathrm{j}^2 = -1$ and $\mathcal{H}(\cdot)$ is the Hilbert transform operator. The ith InA (InA_i) is defined as the absolute value of the analytic function $x_i^a(n)$. The trend of the InA can be used to evaluate atrial activity. The linear regression operator results in the calculation of the trend/slope. The slope is positive for normal sinus rhythm because a P-wave exists. However, for AF, the slope is less steep or even negative due to the lack of a P-wave [8]. In this work, two slope values (denoted β_2 and β_3) are estimated on the basis of InA_2 and InA_3, respectively [8]. The waveforms of InA_2 and InA_3 in the case of non-AF and AF episodes, as well as the corresponding regression lines, are presented in Figure 5.

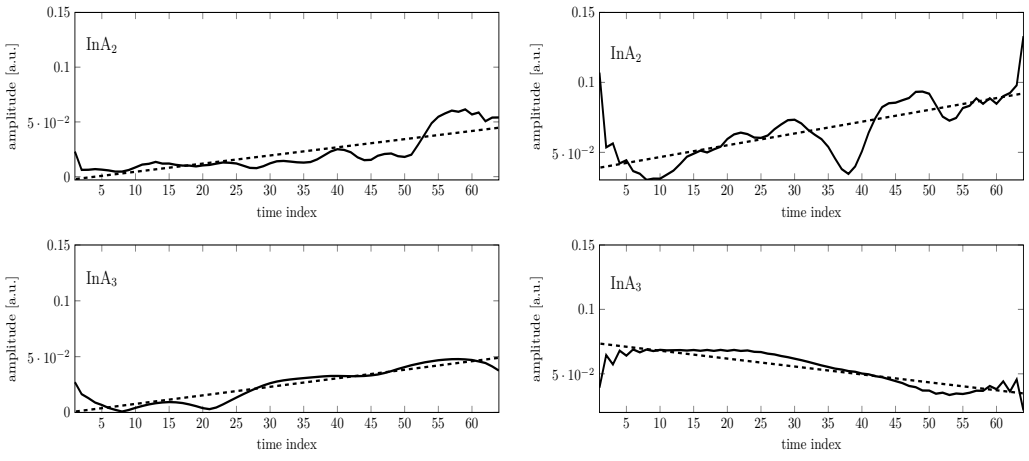

(**a**) (**b**)

Figure 5. Waveforms of InA_2 and InA_3 without AF (**a**) and with AF (**b**); dashed lines denote the regression line.

2.5. Other Parameters Used for Atrial Activity and Heart Rate Evaluation

2.5.1. Turning Point Number

A turning point is a point at which the derivative changes sign, so it may be either a relative maximum or a relative minimum. Determining the number of turning points is a

fast and direct method of assessing the irregularity of the time series, and it is calculated according to the approach presented in ref. [8].

2.5.2. Sample Entropy

The sample entropy (SaEn) belongs to a family of statistics that measure the complexity and regularity of time-series data. The sample entropy is calculated as

$$\text{SaEn} = -\log\left(\frac{A}{B}\right) = \log(B) - \log(A), \tag{11}$$

where A, B is the number of vector pairs matching within a specified tolerance r of their Chebyshev distances [8].

2.5.3. Spectral Entropy and Rényi Entropy

The Spectral Entropy (SpEn) is a measure of the distribution of power in a signal. For the atrial activity signal (P-wave) $x(n)$, the power spectrum is $S(m) = |X(m)|^2$, where $X(m)$ denotes the discrete Fourier transform of $x(n)$. The probability distribution $P(m)$ is given as

$$P(m) = \frac{S(m)}{\sum_i S(i)}. \tag{12}$$

The spectral entropy is then given as

$$\text{SpEn} = -\frac{1}{\log_2 N} \sum_{m=1}^{N} P(m) \log_2 P(m), \tag{13}$$

where N represents all the frequency components. The Matlab function is used to calculate SpEn.

The Rényi entropy is expressed as

$$\text{REN}(\alpha) = -\frac{\alpha}{1-\alpha} \sum_{m=1}^{N} \log_2 (P(m))^{\alpha}, \tag{14}$$

where $\alpha > 0$ and $\alpha \neq 1$; in this work, $\alpha = 2$.

2.5.4. Higuchi's Fractal Dimension (HFD) of Heart Rate

The heart rhythm derived from 30 beats is evaluated with Higuchi's fractal dimension [60]. The discrete signal is expressed as time series $x(1), x(2), \ldots, x(N)$, where $x(i) = \text{RR}_i$. From the starting time sequence, the curve $L_m(k)$ is calculated for each of the time series k as

$$L_m(k) = \frac{1}{k}\left[\left(\sum_{i=1}^{\lfloor \frac{N-m}{k} \rfloor} |x(m+ik) - x(m+(i-1)k)|\right) \frac{N-1}{\lfloor \frac{N-m}{k} \rfloor k}\right], \tag{15}$$

where N is the length of the original time series and $\frac{N-1}{\lfloor \frac{N-m}{k} \rfloor k}$ represents a normalization factor. $L_m(k)$ is then averaged over all m to produce an average curve length value $L(k)$ for each $k = 1, \ldots, k_{\max}$ as [60]

$$L(k) = \frac{1}{k} \sum_{m=1}^{k} L_m(k). \tag{16}$$

The slope of the best linear fit from the plot of ln(L(k)) versus ln(1/k) estimates the HFD.

$$\text{HFD} = \frac{\ln(L(k))}{\ln(1/k)}. \tag{17}$$

2.6. Summary of Features

The features used in this work to detect atrial fibrillation are summarized in Table 1. A set of features is determined for each signal segment containing 30 detected QRS complexes. The segments of the ECG do not overlap. The number of vectors for individual signals from the MIT-BIH AF database varies, but they form a dataset that the classifier uses for its training and testing.

Table 1. Summary of features used in this work.

No.	Parameter	Description	Assessment of
1	HFD	Higuchi fractal dimension	RR intervals
2	HFD_{aa}	Higuchi fractal dimension	Atrial activity part of ECG; value averaged over 30 beats
3	TPN	Turning point number	
4	SaEN	Sample entropy	
5	SpEn	Spectral entropy	
6	REN	Rényi entropy	
7, 8	β_2, β_3	EEMD, slope of the absolute value of the analytic signals InA_2, InA_3	Atrial activity part of ECG, value averaged over 30 beats
9, . . . , 17	$\hat{v}_j^2$	Variance of MODWT, $j = 1, \ldots, 9$	ECG signal containing 30 QRSs
18, 19	$\zeta_{1,2}$	DQ-TQWT, the ratio of the peak energy to the average energy	DQ-TQWT, ECG signal containing 30 QRSs
20, 21	$E_{\mathbf{w}1,\mathbf{w}2}$	Maximum wavelet entropy of $\mathbf{w}_{1,2}$	

The effectiveness of machine learning depends on the empirical data available and the intricacy of the model assumed [4]. For this reason, the wrapper approach is applied in this work for feature selection [61]. Therefore, a genetic algorithm is employed to find the best feature subset. The support vector machine (SVM) classification algorithm is utilized to train and assess the generated feature subsets. The classification performance of the generated subsets is compared in terms of the minimum value of the error classification, and the subset that displays the best performance is selected as the optimum feature subset [61].

2.7. LS-SVM Classifier

The support vector machine (SVM) is one of the best-known methods for data classification. It maintains this popularity due to its effective generalization ability, which results from its risk-minimizing structure [62]. Classification is achieved by a linear or non-linear separating surface in the input space of the dataset [63]. The SVM constructs an optimal separation hyperplane between the positive and negative classes with the maximum margin for binary-class classifications. It can be formulated as a quadratic programming problem that involves inequality constraints. The corresponding class labels are as follows: '−1' denotes the non-atrial-fibrillation class, and '+1' denotes the atrial fibrillation class. The major issue with the SVM is that it requires a large amount of computing power when dealing with datasets containing many dimensions. In this work, a variant of the SVM method is used. The original SVM is altered to reach the optimal solution by resolving a system of linear equations instead of a quadratic programming (QP) problem [64,65]. The least-squares SVM (LS-SVM) was proposed by Suykens et al. [66]. The LS-SVM algorithm optimizes the training process by removing the necessity of solving the quadratic programming problem, providing a more efficient approach. The details of the LS-SVM are discussed in ref. [66].

2.8. Dataset Description

The proposed method was evaluated using the publicly available MIT-BIH Atrial Fibrillation Database (AFDB) of ECGs [67]. The AFDB consists of two-channel ECG signals sampled with a 12-bit resolution in the ±10 mV range. In total, approximately 41% of the

heartbeats are denoted as AF, 57% as NSR, and the rest (1.2%) are from other arrhythmia categories [8]. The AFDB allows for the use of existing annotations of R-peak locations [67]. A sequence of 30 QRS complexes in the ECG signal is labeled as AF if the expert identifies at least half of the beats as AF; otherwise, the 30 QRS complexes are labeled as non-AF. The percentage of segments marked as AF varies (Table 2). The percentage of AF episodes in the data determined by collecting 30 consecutive QRS complexes is very similar to the percentage of AF episodes determined when considering QRS complexes separately, as was shown in ref. [4]. When analyzing the individual signals in Table 2, it can be seen that there is a significant imbalance in the percentage of AF episodes between them; for example, for signal 5091, the percentage of AF is 0.33%, while for 7162 or 7859 it is 100%, and for only one signal (6995) is the percentage of AF close to 50%. In the current study, it was decided to consider all the feature vectors obtained ($N_{AF} + N_{nAF}$ = 37,606) as independent vectors; thus, the overall percentage of AF cases was about 46%. While verifying the performance of the classifier using the *K*-fold cross-validation procedure, it was decided that in each of the training and test subsets created, this proportion should be maintained.

Table 2. The number of analyzed classes described by the number of AF (N_{AF}) and non-AF (N_{nAF}) segment labels and the ratio of AF labels (N_{AF}) to the total number of segments (N_{seg}) for a given signal.

File	Signal											
	4015	**4043**	**4048**	**4126**	**4746**	**4908**	**4936**	**5091**	**5121**	**5261**	**6426**	**6453**
N_{AF}	17	489	27	109	1028	197	1323	4	1129	30	1770	16
N_{nAF}	1449	1574	1304	1319	567	1861	465	1222	533	1487	68	1145
N_{AF}/N_{seg} (%)	1.16	23.70	2.03	7.63	64.45	9.57	79.99	0.33	67.93	1.98	96.30	1.38
File	**Signal**											
	6995	**7162**	**7859**	**7879**	**7910**	**8215**	**8219**	**8378**	**8405**	**8434**	**8455**	**All**
N_{AF}	916	1309	2008	1334	225	1104	475	383	1502	77	1475	16947
N_{nAF}	923	0	0	552	994	341	1501	1134	459	1251	510	20659
N_{AF}/N_{seg} (%)	49.81	100.00	100.00	70.73	18.46	76.40	24.04	25.25	76.6	5.79	74.30	45.06

2.9. Performance Metrics and Experimental Setup

The performance of the AF classification was evaluated by the following quality factors: accuracy (Acc), sensitivity (Sen), specificity (Spec), positive predictivity value (PPV), negative predictivity value (NPV), and F1 score. The factors were calculated on the unseen (testing) dataset using a confusion matrix. These factors are defined, respectively, as

$$\text{Acc} = \frac{TP + TN}{TP + FN + FP + TN}, \tag{18}$$

$$\text{Sen} = \frac{TP}{TP + FN}, \tag{19}$$

$$\text{Spec} = \frac{TN}{FP + TN}, \tag{20}$$

$$\text{PPV} = \frac{TP}{TP + FP}, \tag{21}$$

$$\text{NPV} = \frac{TN}{TN + FN}, \tag{22}$$

$$\text{F1} = \frac{2 \cdot \text{Sen} \cdot \text{PPV}}{\text{Sen} + \text{PPV}}, \tag{23}$$

where TP is true positive, TN is true negative, FP is false positive, and FN is false negative.

The LS-SVM classifier performance was estimated using the cross-validation (CV) statistical method. In this work, all data were validated with a five-fold CV. Using the *K*-fold CV method can help produce an efficient model for imbalanced data. The average performance of the model was calculated on all test sets. The set of parameters for the DQ-TQWT was the following: $Q_1 = 6$, $r_1 = 4$, $J_1 = 45$, $Q_2 = 1$, $r_2 = 4$, $J_2 = 11$. The *modwt* and *modwtvar* procedures started with the wavelet 'db2' and level $L = 12$. After extensive experimentation, this number was determined to produce the optimal results. The parameters of the genetic algorithm in the feature selection method (wrapper method) were as follows: the crossover rate was 0.8, and the mutation rate was 0.01. For SVM-type classification, class labels $\{-1, 1\}$ were assigned to the feature vectors to represent the presence or absence of the AF episode. The input data were scaled to the range $[-1, 1]$ [4,63]. A Matlab 2022b environment (Mathworks, Natick, MA, USA) was used to implement the proposed method. All signal processing and model training and testing procedures for this study were custom programed in Windows 10 on a computer equipped with an AMD(R) AMD Ryzen 7 2700X and 32 GB RAM.

3. Results

3.1. Feature Selection Results

The proposed features were divided into two groups according to whether or not they contained AF. They were then tested to determine their origin from the same population. For this purpose, we used the Mann–Whitney U-test, also known as the Wilcoxon rank sum test, which is a non-parametric statistical test for comparing two samples or groups. This verified whether the groups came from populations with different levels of the variable of interest. From this, it follows that the hypotheses in the Mann–Whitney U-test were:

- **H0.** *The null hypothesis states that the two populations are equal.*
- **H1.** *The alternative hypothesis states that the two populations are not equal.*

A summary of the proposed features during episodes of AF and non-AF is given in Table 3, as well as the results of the Mann–Whitney U-tests. Only for HFD_{aa}, REN, and HFD were there no reasons to reject Hypothesis H0. For the remaining features, hypothesis H0 was rejected, demonstrating the existence of a significant difference in the medians of the two distributions.

This work used the *K*-fold cross-validation method with $K = 5$ to carry out the wrapper method of feature selection, which was performed independently of the LS-SVM model performance test procedure. In this case, each of the five prepared sets of feature vectors served as data for the feature selection method. Then, the feature selection method used only 80% of all feature vectors each time. A genetic algorithm was used to identify the most suitable set of features and executed 10 times for each of the five sets. Overall, this gave 50 different sets of selected features. The objective function of the genetic algorithm was to maximize the prediction accuracy rate, calculated as

$$Acc = \frac{\mathbf{y}_{\text{test}} = \mathbf{y}_{\text{predict}}}{\mathbf{y}_{\text{test}}} \cdot 100[\%], \tag{24}$$

where $\mathbf{y}_{\text{predict}}$ denotes the predicted value of the classifier for the selected set of features, and $\mathbf{y}_{\text{test}}$ is the known test value. For the feature selection process, we were provided with a dataset that contained 80% of all features. This resulted in a dataset of 30,085 vectors for a given number of total cases N = 37,606. Of these, 75% (22,564 feature vectors) were used in the operation of the genetic algorithm. The remaining 25% (7521 vectors) were used to determine the accuracy rate (Acc) of the prediction. The manipulations performed prevented the chosen features from being over-matched to the examined database. The feature selection results are shown in Figure 6. It is evident that features $E_{\mathbf{w}2}$, SpEn, InA_2, Ren, and ζ_1 were the most commonly seen in the set of features that guaranteed the highest value of the classification accuracy factor. On the other hand, it is possible to identify features that appeared less often in the feature sets allowing for high *Acc* accuracy values to be achieved. These features were

HFD_{aa} and HFD, as well as $\hat{v}_i^2$ for $i = 1, 6, 7, 8, 9$. The selected features were very similar to those selected when the reference methods were used, i.e., ReliefF [68,69] and MRMR [68,70]. A comparison of the chosen set of features is displayed in Table 4.

Table 3. Summary characteristics of features used in this work for non-AF and AF, and the results of the Mann–Whitney U-test ($\alpha = 0.01$, $h = 1$ indicates the rejection of the null hypothesis H_0).

	Non-AF		AF			
Feature	**Mean**	**Std**	**Mean**	**Std**	***p*-Value**	**h**
E_{w1}	26.4109	9.8015	20.5394	8.2889	0	1
E_{w2}	23.3416	8.6224	18.7514	9.8648	0	1
β_2	0.0005	0.0005	−0.0001	0.0003	0	1
β_3	0.0004	0.0006	−0.0002	0.0004	0	1
HFD_{aa}	1.1206	0.1257	1.1416	0.1638	0.2572	0
TPN	13.5132	4.1173	13.1830	5.5986	0	1
SpEn	0.9288	0.0044	0.9288	0.0046	0	1
REN	1.6723	1.4262	1.8316	1.8735	0.3374	0
SaEN	0.1471	0.0867	0.1918	0.0984	0	1
HFD	1.9701	0.3028	1.9714	0.1364	0.0007	1
ζ_1	5.8912	2.6763	4.6510	1.5945	0	1
ζ_2	3.3973	0.8831	3.8139	1.2100	0	1
$\hat{v}_1^2$	0.0002	0.0004	0.0002	0.0002	0	1
$\hat{v}_2^2$	0.0017	0.0016	0.0017	0.0019	0	1
$\hat{v}_3^2$	0.0108	0.0101	0.0095	0.0101	0	1
$\hat{v}_4^2$	0.0234	0.0291	0.0198	0.0237	0	1
$\hat{v}_5^2$	0.0254	0.0446	0.0286	0.0452	0	1
$\hat{v}_6^2$	0.0273	0.0689	0.0347	0.0686	0	1
$\hat{v}_7^2$	0.0145	0.0324	0.0196	0.0396	0	1
$\hat{v}_8^2$	0.0021	0.0059	0.0017	0.0033	0	1
$\hat{v}_9^2$	0.0003	0.0025	0.0005	0.0009	0	1

Table 4. Feature importance scores (in descending order) obtained using method proposed in this work and the reference methods ReliefF [68,69] and MRMR [68,70] (the features rejected in the proposed method are highlighted in gray).

No.	**This Work**	**ReliefF [68,69]**	**MRMR [68,70]**
1	E_{w2}	β_2	β_2
2	SpEn	REN	β_3
3	β_2	E_{w2}	$\hat{v}_9^2$
4	REN	β_3	ζ_1
5	ζ_1	ζ_1	SaEn
6	β_3	E_{w1}	E_{w1}
7	ζ_2	ζ_2	E_{w2}
8	$\hat{v}_2^2$	SpEn	TPN
9	E_{w1}	TPN	ζ_2
10	TPN	HFD	$\hat{v}_4^2$
11	SaEN	SaEN	HFD_{aa}
12	$\hat{v}_5^2$	$\hat{v}_5^2$	$\hat{v}_1^2$
13	$\hat{v}_3^2$	$\hat{v}_3^2$	REN
14	$\hat{v}_4^2$	$\hat{v}_2^2$	$\hat{v}_7^2$
15	HFD_{aa}	$\hat{v}_4^2$	$\hat{v}_3^2$
16	$\hat{v}_8^2$	$\hat{v}_8^2$	SpEn
17	$\hat{v}_6^2$	$\hat{v}_7^2$	$\hat{v}_2^2$
18	$\hat{v}_7^2$	$\hat{v}_6^2$	$\hat{v}_8^2$
19	$\hat{v}_1^2$	HFD_{aa}	$\hat{v}_6^2$
20	$\hat{v}_9^2$	$\hat{v}_1^2$	HFD
21	HFD	$\hat{v}_9^2$	$\hat{v}_5^2$

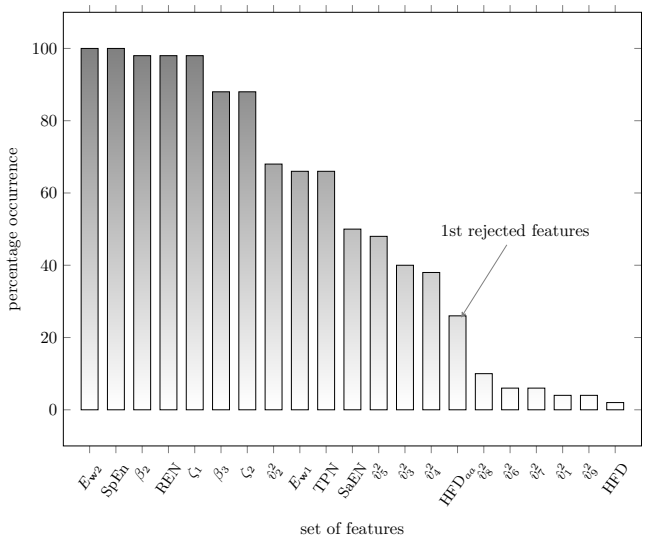

Figure 6. A histogram showing the percentage occurrence of features for the selection feature method based on their accuracy rate (the arrow indicates the first feature that can be ignored, along with those to its right).

Two sets of features are visually compared with t-SNE (t-distributed stochastic neighbor embedding) in Figure 7 [71]. It can be seen that with a complete set of features, the boundaries between the two classes (non-AF and AF cases) often overlapped in many areas, while reducing the number of features to 14 led to the better separation of the two classes.

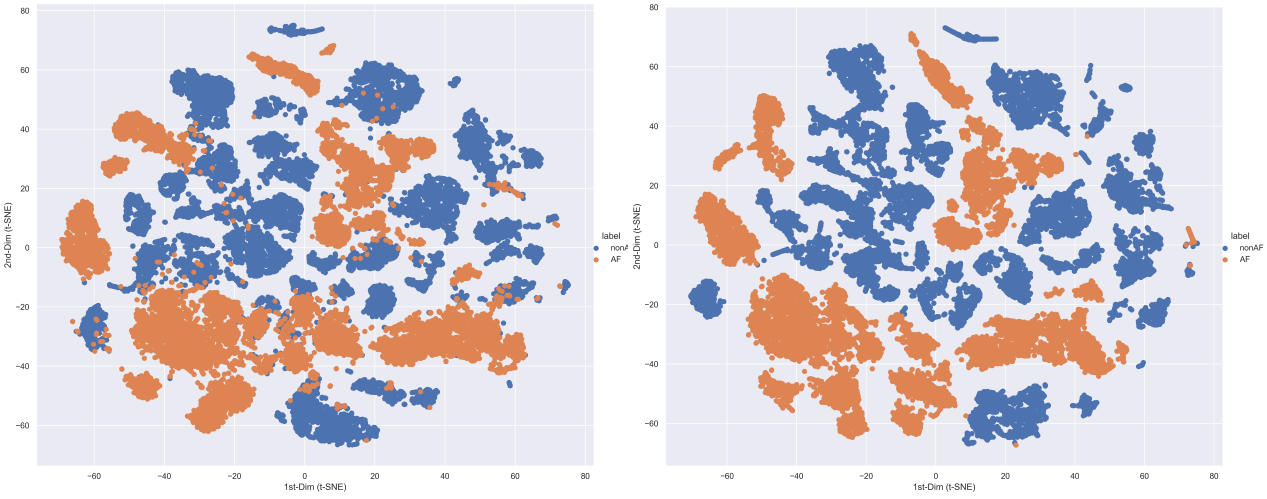

(**a**) A full set of features. (**b**) A reduced set of features.

Figure 7. t-SNE visualization in 2D map for non-AF and AF classes (blue denotes non-AF, orange denotes AF): (**a**) full set of twenty-one features, (**b**) reduced set of fourteen features.

3.2. Performance Evaluation

The proposed method was tested on the AFDB. Table 5 presents the mean and standard deviation for each fold's performance. The proposed method achieved the best results using the LS-SVM classifier with the reduced set of proposed features. However, the differences among the applied classifiers were negligible and fell within the statistical error margin.

Table 6 shows the AF detection results for all ECG signals from the AFDB. The F1 score fluctuated more than in the first part of the tests. In the current version of the proposed method, online (real-time) operation is not foreseen because of the high computational cost of, among other things, the signal transformations used, such as EEMD, DQ-TQWT, and MODWT.

Table 5. Summary of AF detection classification performance using the LS-SVM classifier for standard 5-fold CV; SVM classifiers (kernel: both with the radial Gaussian function—RBF and quadratic function); and the trilayered neural network classifier (NN class).

	This Work (LS-SVM RBF)		SVM RBF		SVM Quadratic		NN Class	
	All Features Mean ± Std	Selected Features Mean ± Std	All Features Mean ± Std	Selected Features Mean ± Std	All Features Mean ± Std	Selected Features Mean ± Std	All Features Mean ± Std	Selected Features Mean ± Std
PPV %	98.74 ± 0.13	98.83 ± 0.11	98.69 ± 0.24	98.64 ± 0.19	97.25 ± 0.07	96.60 ± 0.20	98.16 ± 0.21	98.15 ± 0.19
NPV %	99.07 ± 0.16	99.06 ± 0.20	98.82 ± 0.11	98.94 ± 0.11	97.98 ± 0.15	97.67 ± 0.20	98.46 ± 0.36	98.44 ± 0.17
Sen %	98.87 ± 0.20	98.86 ± 0.24	98.56 ± 0.13	98.71 ± 0.14	97.55 ± 0.19	97.17 ± 0.25	98.25 ± 0.30	98.10 ± 0.21
Spec %	98.96 ± 0.11	99.04 ± 0.09	98.93 ± 0.20	98.88 ± 0.16	97.74 ± 0.06	97.19 ± 0.25	98.40 ±0.22	98.18 ± 0.18
Acc %	98.92 ± 0.12	98.95 ± 0.12	98.76 ± 0.10	98.80 ± 0.12	97.65 ± 0.09	97.18 ± 0.08	98.33 ± 0.17	98.15 ± 0.19
F1 %	98.81 ± 0.13	98.84 ± 0.14	98.63 ± 0.11	98.67 ± 0.14	97.40 ± 0.11	96.88 ± 0.09	98.20 ± 0.13	97.95 ± 0.21

Table 6. Detailed LS-SVM classifier results using the selected set of features (rounded to 2 decimal places; n/a if unavailable).

File	Signal											
	4015	4043	4048	4126	4746	4908	4936	5091	5121	5261	6426	6453
PPV %	76.19	98.16	100.00	94.69	100.00	100.00	99.55	57.14	98.77	100.00	99.72	100.00
NPV %	99.93	99.43	99.92	99.85	100.00	99.95	99.35	100.00	99.05	100.00	100.00	99.91
Sen %	94.12	98.16	96.30	98.17	100.00	99.49	99.77	100.00	99.56	100.00	100.00	93.75
Spec %	99.65	99.43	100.00	99.55	100.00	100.00	98.71	99.75	97.37	100.00	92.65	100.00
Acc %	99.59	99.13	99.92	99.44	100.00	99.95	99.50	99.76	98.86	100.00	99.73	99.91
F1 %	84.21	98.16	98.11	96.40	100.00	99.75	99.66	72.73	99.16	100.00	99.86	96.77
File	**Signal**											
	6995	7162 *	7859 *	7879	7910	8215	8219	8378	8405	8434	8455	
PPV %	100.00	100.00	100.00	99.93	100.00	99.91	98.09	99.22	99.93	98.70	100.00	
NPV %	99.35	n/a	0.00	100.00	99.80	99.71	99.07	99.91	100.00	99.92	99.80	
Sen %	99.34	100.00	99.95	100.00	99.11	99.91	97.05	99.74	100.00	98.70	99.93	
Spec %	100.00	n/a	n/a	99.82	100.00	99.71	99.40	99.74	99.78	99.92	100.00	
Acc %	99.67	100.00	99.95	99.95	99.84	99.86	98.84	99.74	99.95	99.85	99.95	
F1 %	99.67	100.00	99.98	99.96	99.55	99.91	97.57	99.48	99.97	98.70	99.97	

[*] ECG was 100% AF.

4. Discussion

4.1. Study of Selected Features

The feature vector comprised 21 elements, which were defined and described in the preceding sections. These elements could be classified into two groups. The first group consisted of a single non-linear HFD indicator calculated using the heart rate [8]. This indicator changed marginally, and the average values for non-AF and AF episodes were comparable, as indicated in Table 3. However, as reported in ref. [8], the Higuchi fractal dimension calculated over RR intervals had remarkably similar values. It is essential to note that the HFD indicator based on RR intervals could not accurately distinguish non-AF and AF episodes. In ref. [8], it was discovered that the non-linear fractal dimension could be used to assess atrial activity, specifically HFD_{aa}. It is important to note that while both HFD (based on RR intervals) and HFD_{aa} were not included in the reduced set of features (as seen in Figure 6), HFD_{aa} was used more frequently than HFD in almost all optimal sets of features. This was confirmed by the Mann–Whitney U-test (as seen in Table 3). The results showed that there were no significant differences between the AF and non-AF classes for the parameters HFD_{aa} and REN, indicating that the null hypothesis could not be rejected. A similar situation was observed for the HFD feature (p-value greater than 0). When analyzing the accuracy of the feature sets, the REN and SpEn features (which measured the entropy in the atrial activity part of the ECG signal) were found to be significant in the reduced set of features, as shown in Figure 6.

The second group of features was calculated on the basis of the atrial activity segment. Table 3 shows a significant difference in the values β_2 and β_3 between non-AF and AF

episodes. In the case of the occurrence of AF, the values of β_2 and β_3 could be negative, in contrast to the other parameters used. This behavior was similar to that observed in ref. [33]. Non-AF (or NSR) occurrence was characterized by higher positive values than AF episodes. The EEMD methodology was used for the computation of these parameters. However, this makes these parameters unsuitable for online operation due to the considerable computational complexity [57,59]. For the remaining parameters of the second group, the values of the features taken into account were not in ranges that could be clearly defined. Compared to parameters such as HFD_{aa}, SpEn, and HFD, whose range of value variation was very narrow, the variability of values for the rest of the parameters was greater. However, most often, the values that were assigned to the AF class overlapped to some extent with those assigned to the non-AF class. An interesting point of distinction between the classes of atrial fibrillation occurrence and absence was provided by the parameters $E_{\mathbf{w}1}$ and $E_{\mathbf{w}2}$, which are defined as the maximum entropy value (Shannon entropy) in individual sub-bands for the high- and low-resonance components of the DQ-TQWT [10].

The DQ-TQWT produced two ratios, ζ_1 and ζ_2, which measured the ratio of maximum energy to average energy for high- and low-resonance components. Table 3 shows that these two parameters, although presenting overlapping value ranges, could be used to differentiate between AF occurrence and non-occurrence cases. The usefulness of this parameter was further demonstrated by its frequent presence in the feature set that yielded the highest accuracy (see Figure 6). In this case, ζ_1 appeared slightly more often than ζ_2.

The last group of parameters was calculated from the variance of the MODWT. In this study, nine values of $\hat{v}_j^2$ were selected, but not all allowed for an equal contribution to the reduced set of features. The parameters of the most significance were $\hat{v}_2^2$, $\hat{v}_5^2$, $\hat{v}_3^2$, and $\hat{v}_4^2$ (these parameters are listed in descending order of frequency of occurrence in Figure 6).

The TPN parameter proved its usefulness in detecting atrial fibrillation. The results of the Mann–Whitney U-test presented in Table 3 show that there were differences in the value distribution of this parameter for AF and normal-beat distribution for the atrial activity segment in the ECG.

4.2. Quality Assessment of Classification Performance

As mentioned above, three SVM-based classifiers as well as a trilayered neural network were chosen due to their popularity and the possibility of comparing the classification results [4,6,14,30,47]. The training time of the models varied due to the different ways in which the algorithms were implemented. The use of parallel computing capabilities in the Matlab environment could significantly reduce the training time despite the large size of the learning set. The testing procedure was therefore no longer such a problem.

Table 5 reveals that the SVM classifiers with RBF functions achieved the best performance, while the SVM classifiers with a quadratic function produced slightly worse results. This was true for both the complete set of features and the reduced set of features. However, for the SVM method with a quadratic function, the differences were more pronounced when using the reduced set of features, exceeding the standard deviation interval.

The results achieved by the trilayered neural network for both feature sets were comparable to those of the LS-SVM and SVM classifiers (both with RBF), although they were slightly poorer. The LS-SVM method yielded slightly better results when using a reduced feature set, although the standard deviation was also slightly higher. The SVM method with RBF followed a similar pattern. However, the SVM method with a quadratic function produced considerably lower results with the reduced set of features. Notably, using the LS-SVM method with a reduced set of features yielded the most precise classification outcomes. Nevertheless, removing only seven features may not substantially reduce the workload during the classifier's feature selection and learning phases. Moreover, further decreasing the number of features could potentially hinder the classifier's performance.

The results of one of the LS-SVM models that underwent *K*-fold CV training are presented in Table 6. The training set was composed of randomly selected feature vectors from the entire AFDB, and the *K*-fold CV procedure combined both training and test data in a single

record. However, for more realistic, critical, and useful results, individual signals were used as test sets with specific feature vectors determined for each. As seen in Table 6, file 5091 had the smallest F1 measure of 72.73%, while file 4015 had the second smallest F1 score of 84.21%. Most subjects had individual results above 96%. A direct comparison with the results presented in ref. [8] showed that for signals 4015 and 5091 (the worst individual results for AF detection in the sense of the smallest F1 scores), the proposed set of features led to better results. The lowest F1 score here was 72.73%, whereas for reference [8] it was below 30%. Files with a segment ratio of N_{AF}/N_{seg} close to or below unity exhibited the poorest performance, as evidenced by their achievement of the smallest F1 values. This indicated that the AF sections in the AFDB recordings were shorter than others. The values of the PPV ratio (below 80% in both cases) illustrated the difficulty in detecting episodes of AF. However, if the value of the ratio was more significant (such as in file 6453), the F1 index increased to over 96%.

4.3. Comparison with State-of-the-Art Methods

Several methods, including the proposed algorithm, were evaluated for their effectiveness in detecting atrial fibrillation using the MIT-BIH Atrial Fibrillation Database. The evaluation of the methods was conducted with the utmost rigor, taking into account the variations in features, data window size, and other parameters. The assessment was based on the values of the Acc, F1, Sen, Spec, and PPV parameters, which were carefully analyzed to determine the effectiveness of the methods. The results of this comparative analysis can be found in Table 7. This table provides an overview of the work of researchers on AF detection using the MIT-BIH AFDB database and includes the results obtained using SVM methods. In the study by Andersen [26], five time-domain features were proposed for detecting AF based on inter-beat intervals. These features included three entropy-based measures (sample entropy, coefficient of sample entropy, and Shannon entropy) and two measures based on the characteristics of the RR interval (root mean square of successive difference and normalized root mean square of successive difference). It is important to note that the results were obtained using an SVM classifier. The accuracy of the results varied depending on the duration of the time window and the number of beats used. For a 30-second window, the accuracy obtained was 96.98%, while using up to 300 beats resulted in a slightly lower accuracy of 96.45%.

The papers [4,32] proposed using only the heart rhythm signal to gather information. Five features of the heart rhythm signal were used in ref. [32] along with a simple linear classifier. This approach achieved Sen, Spec, PPV, and Acc values of 95.42%, 96.12%, 94.97%, and 95.62%, respectively, for a window width of 130 beats. Czabański's work [4] demonstrated a significant expansion of the HR signal parameter set. The LSVM classifier used in this study produced some of the highest classification results to date, with a sensitivity of 98.94%, specificity of 98.8%, positive predictive value of 98.39%, accuracy of 98.86%, and F1 score of 98.66%. An additional aggregation stage was included in the research to provide even more reliable information on patient risk. It is worth noting that Czabański's work [4] used a Lagrangian SVM classifier instead of the LS-SVM classifier utilized in our approach.

In the work of Andersen et al. [27], a multi-layer deep learning network featuring convolutional and recurrent layers was used to extract high-level features from segments of RR intervals. This method had a sensitivity of 98.98% and specificity of 96.95% and was validated through a five-fold CV procedure. The great benefit of this approach was that it necessitated a small computational effort, allowing 24-hour ECG recordings to be processed in less than a second. However, its positive predictive value (PPV) of 95.76% was lower than the proposed method's result. In another study, Liaqat et al. [30] proposed the use of long short-term memory (LSTM) and a CNN, but the results were much worse than those obtained with the proposed method, with an F1 score of 86%. A similar approach was proposed in ref. [39]. However, the obtained sensitivity and specificity were 97.87% and 99.29%, respectively. This specificity value is the highest in our comparison. However, the F1 score was lower than the highest value achieved by the proposed method. The results achieved were among the lowest presented in this summary (F1 = 86%). The features obtained from two-lead ECG recordings were processed with the wavelet packet transform, and the random process theory

was used to provide efficient feature selection. A neural network was used as a classifier. The sensitivity and specificity obtained were 98.7% and 98.9%, respectively, representing some of the best values to date [2]. The lightweight 1D CNN model proposed in ref. [42] achieved outstanding results in AF detection, but the performance varied depending on the data length. The undoubted advantage of this solution was the short computation time, but this resulted in lower values for the specificity parameter (95.30%, 93.23%, and 93.99%) compared to other methods, including the method proposed in this work.

In the last two to three years, the features characterizing the RR intervals and the atrial activity part of the ECG signal have yielded promising results for detecting AF. Hu [10] proposed a decision tree classifier that achieved the highest specificity (99.6%) in our comparison but displayed a lower sensitivity (97.9%). Hirsh [8] proposed a hybrid approach that combined the non-linear entropy features of RR intervals and atrial activity, which proved to be superior to approaches that used only one field of analysis. Zhang [46] used a dual-domain attention cascade deep learning method (D2AFNet) to extract and fuse features from segmented ECG signals. With a 10-fold cross-validation procedure, the sensitivity and specificity achieved were 98.39% and 98.57%, respectively, which are among the best values presented here. Based on the overview provided, it is evident that the method proposed in this work accurately detected atrial fibrillation with minimal error. When compared to other non-deep-learning methods outlined in Table 7, the proposed algorithm achieved similar or even better results.

Table 7. A summary of published results for existing AF detection methods using the MIT-BIH Atrial Fibrillation Database in comparison to the proposed work (n/a—not available; the best results are in bold).

Method	Features	Window	Classifiers	Results (%)				
				Sen	Spec	PPV	Acc	F1
Andersen et al., 2017 [26]	RR interval ECG features	300 beats 30 s	SVM	96.81 94.27	96.20 98.84	n/a	96.45 96.98	n/a
Wróbel et al., 2018 [32]	HR irregularity features	21	Linear classifier	95.42	96.12	94.97	95.62	n/a
Kalidas et al., 2019 [22]	RR intervals, Markov matrix	60 s	RF	97.7	98.5	n/a	n/a	97.7
Andersen et al., 2019 [27]	RR interval	10 s	CNN-LSTM	98.98	96.95	95.76	97.8	n/a
Czabański et al., 2019 [4]	HR irregularity features	21 beats	LSVM	98.94	98.80	98.39	98.86	98.66
Hu et al., 2020 [10]	Frequency features	5 s	decision tree	97.9	99.6	n/a	n/a	n/a
Liaqat et al., 2020 [30]	83 RR and ECG features	10 s	LSTM	85.0	n/a	86.0	86.5	86.0
Wang et al., 2020 [2]	Signal	10 s	ANN	98.7	98.9	n/a	98.8	n/a
Hirsh et al., 2021 [8]	RR intervals AA features	30 beats	RF	98.00	97.4	n/a	97.6	97.1
Petmezas et al., 2021 [39]	Signal	187 samples around R-peak	CNN-LSTM	97.87	99.29	n/a	n/a	n/a
Zhang et al., 2023 [46]	Signal	10 s	D2AFNet	98.39	98.57	**99.19**	98.45	98.78
Phukan et al., 2023 [42]	Signal	5 s 10 s 30 s	1D-CNN	99.26 **99.72** 98.57	95.30 93.23 93.99	n/a	97.68 97.50 96.70	n/a
Proposed method, 2023	RR interval AA features	30 beats	LS-SVM	98.86	98.96	99.04	**98.95**	**98.84**

5. Conclusions

Atrial fibrillation is a condition that can have dangerous consequences for patients' health if left undetected. Diagnosing this type of arrhythmia requires the long-term monitoring of the heart, e.g., recording an ECG signal. Episodes of atrial fibrillation may be short and sporadic, making them difficult to detect. However, using automatic AF detection methods in the ECG signal can improve the AF detection performance in long-term signals. This study proposed and evaluated a novel and reliable method for detecting atrial fibrillation episodes in long-term ECG signals. Three signal decomposition techniques were used in this study, i.e., the dual-Q tunable-Q wavelet transform, ensemble empirical mode decomposition, and the corresponding analysis of variance from the maximum overlap discrete wavelet transform. Various features were proposed, including one extracted from the heart rate and others defined based on the segment of atrial activity in the ECG signal after decomposition

with the abovementioned transforms. The LS-SVM classifier was applied with a five-fold cross-validation procedure, outperforming other automatic AF detection methods proposed in the literature. According to the numerical experiments, the first two transformations (DQ-TQWT and EEMD) were the most useful for AF detection. The parameters obtained from these experiments were essential components of a vector of features describing atrial activity in AF detection. Feature selection was also performed such that the selected subset of features provided the same or even better AF detection results than the complete set of features. The algorithm achieved a high accuracy, sensitivity, specificity, PPV, and F1 score, making it suitable for clinical applications. Individual ECG recordings were also classified and compared with the results of the five-fold CV method. In this case, the classification results were better than those presented in the literature, proving the proposed method's high effectiveness in detecting atrial fibrillation. The model can work efficiently with test samples of any length, making it more applicable in clinical settings.

When developing this method, it is worth considering the ratio of AF events to total AF plus non-AF events. A classifier with too few AF events will be unable to identify AF episodes correctly. However, exceeding the specified lower limit of the abovementioned coefficient would mean an AF episode detection rate of almost 100%. Reducing irrelevant features would lead to a better understanding of which features to focus on to achieve even better AF detection and interpretability by medical staff. Due to computational limitations, the proposed method is currently more suitable for offline ECG analysis than implementation in real-time systems. For new data, the derived model needs to be updated. Future research will focus on improving its performance by appropriately selecting the parameters of the LS-SVM classifier; improving the ECG pre-processing step; and, where possible, using more ECG channels.

Funding: This research was supported by statutory funds (BK-235/RAU10/2023) of the Department of Cybernetics, Nanotechnology and Data Processing of the Faculty of Automatic Control, Electronics and Computer Science, Silesian University of Technology, Gliwice, Poland.

Institutional Review Board Statement: Not applicable.

Informed Consent Statement: Not applicable.

Data Availability Statement: The data presented in this study are available on request from the corresponding author. The data are not publicly available due to it is not fully prepared and enabled to share in the repository. The MIT-BIH Atrial Fibrillation Database used in this study are publicly available. This data can be found here: https://physionet.org/content/afdb/1.0.0/ (accessed on 21 October 2023).

Conflicts of Interest: The author declares no conflict of interest.

Abbreviations

The following abbreviations are used in this manuscript:

AA	Atrial activity
AF	Atrial fibrillation
AFDB	Atrial Fibrillation Database
CNN	Convolutional neural network
DQ-TQWT	Dual-Q tunable Q-factor wavelet transform
ECG	Electrocardiogram
EMD	Empirical mode decomposition
EEMD	Ensemble empirical mode decomposition
LS-SVM	Least-squares support vector machine
LSTM	Long short-term memory
MODWT	Maximal overlap discrete wavelet transform
NSR	Normal sinus rate
SVM	Support vector machine
TPN	Turning point number
WT	Wavelet transform

References

1. Vaduganathan, M.; Mensah, G.A.; Turco, J.V.; Fuster, V.; Roth, G.A. The Global Burden of Cardiovascular Diseases and Risk. *J. Am. Coll. Cardiol.* **2022**, *80*, 2361–2371. [CrossRef] [PubMed]
2. Wang, J.; Wang, P.; Wang, S. Automated Detection of Atrial Fibrillation in ECG Signals Based on Wavelet Packet Transform and Correlation Function of Random Process. *Biomed. Signal Process. Control* **2020**, *55*, 101662. [CrossRef]
3. Zhou, X.; Ding, H.; Ung, B.; Pickwell-MacPherson, E.; Zhang, Y. Automatic online detection of atrial fibrillation based on symbolic dynamics and Shannon entropy. *Biomed. Eng. Online* **2014**, *13*, 18. [CrossRef]
4. Czabański, R.; Horoba, K.; Wróbel, J.; Matonia, A.; Martinek, R.; Kupka, T.; Jeżewski, M.; Kahankova, R.; Jeżewski, J.; Łęski, J.M. Detection of Atrial Fibrillation Episodes in Long-Term Heart Rhythm Signals Using a Support Vector Machine. *Sensors* **2020**, *20*, 765. [CrossRef] [PubMed]
5. Liaqat, S.; Dashtipour, K.; Zahid, A.; Arshad, K.; Ullah, J.S.; Assaleh, K.T.; Ramzan, N. A Review and Comparison of the State-of-the-Art Techniques for Atrial Fibrillation Detection and Skin Hydration. *Front. Commun. Netw.* **2021**, *2*, 679502. [CrossRef]
6. Rizwan, A.; Zoha, A.; Mabrouk, I.B.; Sabbour, H.M.; Al-Sumaiti, A.S.; Alomainy, A.; Imran, M.A.; Abbasi, Q.H. A Review on the State of the Art in Atrial Fibrillation Detection Enabled by Machine Learning. *IEEE Rev. Biomed. Eng.* **2020**, *14*, 219–239. [CrossRef]
7. Giraldo-Guzmán, J.; Kotas, M.; Castells, F.; Contreras-Ortiz, S.H.; Urina-Triana, M. Estimation of PQ Distance Dispersion for Atrial Fibrillation Detection. *Comput. Methods Programs Biomed.* **2021**, *208*, 106167. [CrossRef]
8. Hirsch, G.; Jensen, S.H.; Poulsen, E.S.; Puthusserypady, S. Atrial Fibrillation Detection Using Heart Rate Variability and Atrial Activity: A Hybrid Approach. *Expert Syst. Appl.* **2021**, *169*, 114452. [CrossRef]
9. Weng, B.; Wang, J.J.; Michaud, F.; Blanco-Velasco, M. Atrial Fibrillation Detection Using Stationary Wavelet Transform Analysis. In Proceedings of the 30th Annual International Conference of the IEEE Engineering in Medicine and Biology Society, Vancouver, BC, Canada, 20–25 August 2008; pp. 1128–1131. [CrossRef]
10. Hu, Y.; Zhao, Y.; Liu, J.; Pang, J.; Zhang, C.; Li, P. An Effective Frequency-Domain Feature of Atrial Fibrillation Based on Time–Frequency Analysis. *BMC Med. Inform. Decis. Mak.* **2020**, *20*, 308. [CrossRef]
11. Neri, L.; Oberdier, M.T.; Van Abeelen, K.C.J.; Menghini, L.; Tumarkin, E.; Tripathi, H.; Jaipalli, S.; Orro, A.; Paolocci, N.; Gallelli, I.; et al. Electrocardiogram Monitoring Wearable Devices and Artificial-Intelligence-Enabled Diagnostic Capabilities: A Review. *Sensors* **2023**, *23*, 4805. [CrossRef]
12. Bahrami Rad, A.; Galloway, C.; Treiman, D.; Xue, J.; Li, Q.; Sameni, R.; Albert, D.; Clifford, G.D. Atrial Fibrillation Detection in Outpatient Electrocardiogram Monitoring: An Algorithmic Crowdsourcing Approach. *PLoS ONE* **2021**, *16*, e0259916. [CrossRef]
13. Mäkynen, M.; Ng, G.; Li, X.; Schlindwein, F. Wearable Devices Combined with Artificial Intelligence—A Future Technology for Atrial Fibrillation Detection? *Sensors* **2022**, *22*, 8588. [CrossRef] [PubMed]
14. Wei, T.-R.; Lu, S.; Yan, Y. Automated Atrial Fibrillation Detection with ECG. *Bioengineering* **2022**, *9*, 523. [CrossRef] [PubMed]
15. Verberk, W.J.; Omboni, S.; Kollias, A.; Stergiou, G.S. Screening for Atrial Fibrillation with Automated Blood Pressure Measurement: Research Evidence and Practice Recommendations. *Int. J. Cardiol.* **2016**, *203*, 465–473. [CrossRef]
16. Bonomi, A.; Schipper, F.; Eerikainen, L.; Margarito, J.; Aarts, R.; Babaeizadeh, S.; De Morree, H.; Dekker, L. Atrial Fibrillation Detection Using Photo: Plethysmography and Acceleration Data at the Wrist. In Proceedings of the Computing in Cardiology Conference 2016, Vancouver, BC, Canada, 11–14 September 2016. [CrossRef]
17. Väliaho, E.-S.; Kuoppa, P.; Lipponen, J.A.; Hartikainen, J.E.; Jäntti, H.; Rissanen, T.T.; Kolk, I.; Pohjantähti-Maaroos, H.; Castren, M.; Halonen, J.; et al. Wrist Band Photoplethysmography Autocorrelation Analysis Enables Detection of Atrial Fibrillation without Pulse Detection. *Front. Physiol.* **2021**, *12*, 654555. [CrossRef] [PubMed]
18. Jiang, F.; Zhou, Y.; Ling, T.; Zhang, Y.; Zhu, Z. Recent Research for Unobtrusive Atrial Fibrillation Detection Methods Based on Cardiac Dynamics Signals: A Survey. *Sensors* **2021**, *21*, 3814. [CrossRef]
19. Nuryani, N.; Harjito, B.; Yahya, I.; Lestari, A. Atrial fibrillation detection using support vector machine. In Proceedings of the Joint International Conference on Electric Vehicular Technology and Industrial, Mechanical, Electrical and Chemical Engineering 2015, Surakarta, Indonesia, 4–5 November 2015; pp. 215–218. [CrossRef]
20. Colloca, R.; Johnson, A.E.; Mainardi, L.; Cliford, G.D. A support vector machine approach for reliable detection of atrial fibrillation events. In Proceedings of the Computing in Cardiology 2013, Zaragoza, Spain, 22–25 September 2013; pp. 1047–1050.
21. Zhou, X.; Ding, H.; Wu, W.; Zhang, Y. A Real-Time Atrial Fibrillation Detection Algorithm Based on the Instantaneous State of Heart Rate. *PLoS ONE* **2015**, *10*, e0136544. [CrossRef]
22. Kalidas, V.; Tamil, L.S. Detection of atrial fibrillation using discrete-state Markov models and Random Forests. *Comput. Biol. Med.* **2019**, *113*, 103386. [CrossRef]
23. Wang, Y.; Liu, S.; Jia, H.; Deng, X.; Li, C.; Wang, A.; Yang, C. A two-step method for paroxysmal atrial fibrillation event detection based on machine learning. *Math. Biosci. Eng.* **2022**, *19*, 9877–9894. [CrossRef]
24. García, M.; Ródenas, J.; Alcaraz, R.; Rieta, J.J. Application of the relative wavelet energy to heart rate independent detection of atrial fibrillation. *Comput. Methods Programs Biomed.* **2016**, *131*, 157–168. [CrossRef]
25. Asgari, S.; Mehrnia, A.; Moussavi, M. Automatic detection of atrial fibrillation using stationary wavelet transform and support vector machine. *Comput. Biol. Med.* **2015**, *60*, 132–142. [CrossRef] [PubMed]

26. Andersen, R.S.; Poulsen, E.S.; Puthusserypady, S. A novel approach for automatic detection of Atrial Fibrillation based on Inter Beat Intervals and Support Vector Machine. In Proceedings of the 39th Annual International Conference of the IEEE Engineering in Medicine and Biology Society (EMBC) 2017, Jeju Island, Republic of Korea, 11–15 July 2017; pp. 2039–2042. [CrossRef]
27. Andersen, R.S.; Peimankar, A.; Puthusserypady, S. A deep learning approach for real-time detection of atrial fibrillation. *Expert Syst. Appl.* **2019**, *115*, 65–473. [CrossRef]
28. Xia, Y.; Wulan, N.; Wang, K.; Zhang, H. Detecting atrial fibrillation by deep convolutional neural networks. *Comput. Biol. Med.* **2018**, *93*, 84–92. [CrossRef] [PubMed]
29. Warrick, P.A.; Nabhan Homsi, M. Ensembling Convolutional and Long Short-Term Memory Networks for Electrocardiogram Arrhythmia Detection. *Physiol. Meas.* **2018**, *39*, 114002. [CrossRef] [PubMed]
30. Liaqat, S.; Dashtipour, K.; Zahid, A.; Assaleh, K.; Arshad, K.; Ramzan, N. Detection of Atrial Fibrillation Using a Machine Learning Approach. *Information* **2020**, *11*, 549. [CrossRef]
31. Chen, X.; Cheng, Z.; Wang, S.; Lu, G.; Xv, G.; Liu, Q.; Zhu, X. Atrial Fibrillation Detection Based on Multi-Feature Extraction and Convolutional Neural Network for Processing ECG Signals. *Comput. Methods Programs Biomed.* **2021**, *202*, 106009. [CrossRef]
32. Wróbel, J.; Horoba, K.; Matonia, A.; Kupka, T.; Henzel, N.; Sobotnicka, E. Optimizing the Automated Detection of Atrial Fibrillation Episodes in Long-Term Recording Instrumentation. In Proceedings of the 25th International Conference "Mixed Design of Integrated Circuits and System" (MIXDES), Gdynia, Poland, 21–23 June 2018; pp. 460–464. [CrossRef]
33. Pal, S.; Maji, U.; Mitra, M. Characterizing Atrial Fibrillation in Empirical Mode Decomposition Domain. *J. Med. Biol. Eng.* **2016**, *36*, 693–703. [CrossRef]
34. Hidalgo-Munoz, A.R.; Tome, A.M.; Zarzoso, V. Empirical Mode Decomposition for Noninvasive Atrial Fibrillation Dominant Frequency Estimation. In Proceedings of the 23rd European Signal Processing Conference (EUSIPCO), Nice, France, 31 August–4 September 2015; pp. 2581–2585. [CrossRef]
35. Rahul, J.; Sharma, L.D. Artificial Intelligence-Based Approach for Atrial Fibrillation Detection Using Normalised and Short-Duration Time-Frequency ECG. *Biomed. Signal Process. Control* **2022**, *71*, 103270. [CrossRef]
36. Katz, M.J. Fractals and the analysis of waveforms. *Comput. Biol. Med.* **1988**, *18*, 145–156. [CrossRef]
37. Bernal-Oñate, C.-P.; Carrera, E.V.; Melgarejo-Meseguer, F.-M.; Gordillo-Orquera, R.; Garcí-A-Alberola, A.; Rojo-álvarez, J.L. Atrial Fibrillation Detection with Spectral Manifolds in Low-Dimensional Latent Spaces. *IEEE Access* **2023**, *11*, 103364–103376. [CrossRef]
38. Padmavathi, K.; Ramakrishna, K.S. Classification of ECG Signal during Atrial Fibrillation Using Autoregressive Modeling. *Procedia Comput. Sci.* **2015**, *46*, 53–59. [CrossRef]
39. Petmezas, G.; Haris, K.; Stefanopoulos, L.; Kilintzis, V.; Tzavelis, A.; Rogers, J.A.; Katsaggelos, A.K.; Maglaveras, N. Automated Atrial Fibrillation Detection Using a Hybrid CNN-LSTM Network on Imbalanced ECG Datasets. *Biomed. Signal Process. Control* **2021**, *63*, 102194. [CrossRef]
40. Staffini, A.; Svensson, T.; Chung, U.; Svensson, A.K. A Disentangled VAE-BiLSTM Model for Heart Rate Anomaly Detection. *Bioengineering* **2023**, *10*, 683. [CrossRef] [PubMed]
41. Nurmaini, S.; Tondas, A.E.; Darmawahyuni, A.; Rachmatullah, M.N.; Umi Partan, R.; Firdaus, F.; Tutuko, B.; Pratiwi, F.; Juliano, A.H.; Khoirani, R. Robust Detection of Atrial Fibrillation from Short-Term Electrocardiogram Using Convolutional Neural Networks. *Future Gener. Comput. Syst.* **2020**, *113*, 304–331. [CrossRef]
42. Phukan, N.; Manikandan, M.S.; Pachori, R.B. AFibri-Net: A Lightweight Convolution Neural Network Based Atrial Fibrillation Detector. *IEEE Trans. Circuits Syst. I* **2023**, 1–13. [CrossRef]
43. Plesinger, F.; Nejedly, P.; Viscor, I.; Halamek, J.; Jurak, P. Automatic Detection of Atrial Fibrillation and Other Arrhythmias in Holter ECG Recordings Using PQRS Morphology and Rhythm Features. In Proceedings of the Computing in Cardiology Conference 2017, Rennes, France, 24–27 September 2017. [CrossRef]
44. Kamaleswaran, R.; Mahajan, R.; Akbilgic, O. A Robust Deep Convolutional Neural Network for the Classification of Abnormal Cardiac Rhythm Using Single Lead Electrocardiograms of Variable Length. *Physiol. Meas.* **2018**, *39*, 035006. [CrossRef]
45. Huerta, Á.; Martinez, A.; Carneiro, D.; Bertomeu-González, V.; Rieta, J.J.; Alcaraz, R. Comparison of Supervised Learning Algorithms for Quality Assessment of Wearable Electrocardiograms with Paroxysmal Atrial Fibrillation. *IEEE Access* **2023**, *11*, 106126–106140. [CrossRef]
46. Zhang, P.; Ma, C.; Song, F.; Sun, Y.; Feng, Y.; He, Y.; Zhang, T.; Zhang, G. D2AFNet: A Dual-Domain Attention Cascade Network for Accurate and Interpretable Atrial Fibrillation Detection. *Biomed. Signal Process. Control* **2023**, *82*, 104615. [CrossRef]
47. Jahan, M.S.; Mansourvar, M.; Puthusserypady, S.; Wiil, U.K.; Peimankar, A. Short-Term Atrial Fibrillation Detection Using Electrocardiograms: A Comparison of Machine Learning Approaches. *Int. J. Med. Inform.* **2022**, *163*, 104790. [CrossRef]
48. Pander, T. A New Approach to Adaptive Threshold Based Method for QRS Detection with Fuzzy Clustering. *Biocybern. Biomed. Eng.* **2022**, *42*, 404–425. [CrossRef]
49. Henriques, T.; Ribeiro, M.; Teixeira, A.; Castro, L.; Antunes, L.; Costa-Santos, C. Nonlinear Methods Most Applied to Heart-Rate Time Series: A Review. *Entropy* **2020**, *22*, 309. [CrossRef] [PubMed]
50. Kumar, A.; Prakash, A.; Kumar, R. Tunable Q-Factor Wavelet Transform for Extraction of Weak Bursts in the Vibration Signal of an Angular Contact Bearing. *Procedia Technol.* **2016**, *25*, 838–845. [CrossRef]
51. Selesnick, I.W. Wavelet Transform with Tunable Q-Factor. *IEEE Trans. Signal Process.* **2011**, *59*, 3560–3575. [CrossRef]

52. Liu, J.; Zhang, C.; Zhu, Y.; Ristaniemi, T.; Parviainen, T.; Cong, F. Automated Detection and Localization System of Myocardial Infarction in Single-Beat ECG Using Dual-Q TQWT and Wavelet Packet Tensor Decomposition. *Comput. Methods Programs Biomed.* **2020**, *184*, 105120. [CrossRef]
53. Selesnick, I.W. Resonance-Based Signal Decomposition: A New Sparsity-Enabled Signal Analysis Method. *Signal Process.* **2011**, *91*, 2793–2809. [CrossRef]
54. Rodrigues, D.V.Q.; Zuo, D.; Li, C. A MODWT-Based Algorithm for the Identification and Removal of Jumps/Short-Term Distortions in Displacement Measurements Used for Structural Health Monitoring. *IoT* **2021**, *3*, 60–72. [CrossRef]
55. Shrifan, N.H.M.M.; Akbar, M.F.; Mat Isa, N.A. Maximal Overlap Discrete Wavelet-Packet Transform Aided Microwave Nondestructive Testing. *NDT & E Int.* **2021**, *119*, 102414. [CrossRef]
56. Gurumoorthy, S.; Babu Muppalaneni, N.; Sandhya Kumari, G. EEG Signal Denoising Using Haar Transform and Maximal Overlap Discrete Wavelet Transform (MODWT) for the Finding of Epilepsy. In *Epilepsy—Update on Classification, Etiologies, Instrumental Diagnosis and Treatment*; Misciagna, S., Ed.; IntechOpen: London, UK, 2021. [CrossRef]
57. Huang, N.E.; Shen, Z.; Long, S.R.; Wu, M.C.; Shih, H.H.; Zheng, Q.; Yen, N.-C.; Tung, C.C.; Liu, H.H. The Empirical Mode Decomposition and the Hilbert Spectrum for Nonlinear and Non-Stationary Time Series Analysis. *Proc. R. Soc. Lond. A* **1998**, *454*, 903–995. [CrossRef]
58. Zhang, J.; Feng, F.; Marti-Puig, P.; Caiafa, C.F.; Sun, Z.; Duan, F.; Solé-Casals, J. Serial-EMD: Fast empirical mode decomposition method for multi-dimensional signals based on serialization. *Inf. Sci.* **2021**, *581*, 215–232. [CrossRef]
59. Huang, N.E. Introduction to the Hilbert-Huang Transform and its related mathematical problems. In *Interdisciplinary Mathematical Sciences*; World Scientific: Singapore, 2005; Volume 5, pp. 1–26, ISBN 978-981-256-376-7. [CrossRef]
60. Kesić, S.; Spasić, S.Z. Application of Higuchi's Fractal Dimension from Basic to Clinical Neurophysiology: A Review. *Comput. Methods Programs Biomed.* **2016**, *133*, 55–70. [CrossRef]
61. Remeseiro, B.; Bolon-Canedo, V. A Review of Feature Selection Methods in Medical Applications. *Comput. Biol. Med.* **2019**, *112*, 103375. [CrossRef] [PubMed]
62. Vapnik, V. The Support Vector Method of Function Estimation. In *Nonlinear Modeling*; Suykens, J.A.K., Vandewalle, J., Eds.; Springer: Boston, MA, USA, 1998; pp. 55–85, ISBN 978-1-4613-7611-8. [CrossRef]
63. Mangasarian, O.L.; Musicant, D.R. Lagrangian Support Vector Machines. *J. Mach. Learn. Res.* **2001**, *1*, 161–177. [CrossRef]
64. Tsujinishi, D.; Abe, S. Fuzzy Least Squares Support Vector Machines for Multiclass Problems. *Neural Netw.* **2003**, *16*, 785–792. [CrossRef] [PubMed]
65. Adankon, M.M.; Cheriet, M.; Biem, A. Semisupervised Learning Using Bayesian Interpretation: Application to LS-SVM. *IEEE Trans. Neural Netw.* **2011**, *22*, 513–524. [CrossRef] [PubMed]
66. Suykens, J.A.K.; Vandewalle, J. Least Squares Support Vector Machine Classifiers. *Neural Process. Lett.* **1999**, *9*, 293–300. [CrossRef]
67. Moody, G.B.; Mark, R.G. A new method for detecting atrial fibrillation using R-R intervals. *Comput. Cardiol.* **1983**, *10*, 227–230.
68. Roffo, G. Ranking to Learn and Learning to Rank: On the Role of Ranking in Pattern Recognition Applications. *arXiv* **2017**, arXiv:1706.05933. [CrossRef]
69. Urbanowicz, R.J.; Meeker, M.; La Cava, W.; Olson, R.S.; Moore, J.H. Relief-Based Feature Selection: Introduction and Review. *J. Biomed. Inform.* **2018**, *85*, 189–203. [CrossRef]
70. Zhao, Z.; Anand, R.; Wang, M. Maximum Relevance and Minimum Redundancy Feature Selection Methods for a Marketing Machine Learning Platform. In Proceedings of the IEEE International Conference on Data Science and Advanced Analytics (DSAA), Washington, DC, USA, 5–8 October 2019; pp. 442–452. [CrossRef]
71. Maaten, L.V.; Hinton, G.E. Visualizing Data using t-SNE. *J. Mach. Learn. Res.* **2008**, *9*, 2579–2605.

Disclaimer/Publisher's Note: The statements, opinions and data contained in all publications are solely those of the individual author(s) and contributor(s) and not of MDPI and/or the editor(s). MDPI and/or the editor(s) disclaim responsibility for any injury to people or property resulting from any ideas, methods, instructions or products referred to in the content.